HYDROGEN PASSIVATION AND PHOSPHOROUS GETTERING AT DIFFERENT GRAIN BOUNDARY TYPES IN MULTICRYSTALLINE SILICON

P. Karzel[1], M. Ackermann[1], L. Gröner[1], C. Reimann[2], M. Zschorsch[3], S. Meyer[4], G. Hahn[1]
[1]University of Konstanz, Department of Physics, 78464 Konstanz, Germany
[2]Fraunhofer IISB, Schottkystr. 10, 91058 Erlangen, Germany
[3]Fraunhofer THM, Am-St.Niclas-Schacht 13, 09599 Freiberg, Germany
[4]Fraunhofer CSP, Walter-Hülse-Str. 1, 06120 Halle, Germany

ABSTRACT: The dependency of minority charge carrier lifetime values at grain boundaries in multicrystalline silicon of different qualities on the grain boundary type after $POCl_3$ gettering and/or firing of SiN_x:H layers deposited by plasma enhanced chemical vapor deposition is analyzed. A new method to determine the coincidence site lattice grain boundary types on large scale is combined with spatially resolved lifetime-calibrated photoluminescence measurements and mappings of the interstitial iron concentration. Lifetime contrast values are calculated. A broader statistics than in former investigations is generated by this approach.
Based on broad statistics, a dependency of the efficacy of all applied processes on the grain boundary type is shown -: higher coincidence site lattice indexes correlate with a decrease of median lifetime values after all applied processes. Hydrogenation of grain boundaries is found to be more effective in cleaner samples. The lifetime contrast values are dependent on the degree of contamination of the multicrystalline silicon material. In less contaminated samples they rather decrease after the processes, whereas in standard solar-grade material they increase after $POCl_3$ diffusion and decrease again after subsequent hydrogenation. No correlation with the interstitial iron concentration could be found.
Keywords: multicrystalline silicon, grain boundaries, minority charge carrier lifetime, grain boundary type

1 INTRODUCTION

In comparison to monocrystalline silicon wafers, mc-Si wafer quality is lowered by higher impurity concentration, grain boundaries and dislocations. As a consequence, the minority charge carrier lifetimes in as-cut wafers are lower. During standard solar cell production processes like $POCl_3$ diffusion for emitter formation and hydrogenation of the wafer bulk by firing of hydrogen-rich SiN_x:H layers deposited by plasma enhanced chemical vapor deposition (PECVD) average lifetime values can be significantly enhanced [1,2].

In contrast, the *local* effect of the two processes to *grain boundaries* in material with high impurity concentration can be different. As grain boundaries are heavily decorated by transition metal precipitates that dissolve during high temperature processes like e.g. $POCl_3$ diffusion and decorate grain boundaries with dissolved metal impurities [3,4], the lifetime can be locally decreased at grain boundaries after P-gettering [5]. Additionally, metal impurities diffusing through the crystal during $POCl_3$ diffusion are attracted by grain boundaries that act as getter sinks. After such a possible decrease of lifetime during $POCl_3$ diffusion, it can be increased again by subsequent hydrogenation. The net change in minority charge carrier lifetime after the two processes can be still positive at some grain boundaries, but the improvement can be rather small [5] and differs [6]. In prior investigations a possible correlation between the coincidence site lattice (CSL) grain boundary type and the efficacy of a passivation of the recombination activity by H at different CSL grain boundaries was indicated [6-12]. The statistics in all of these analyses could only be derived from measurements at a small number of grain boundaries, because the CSL grain boundary types were determined with the microscopic analysis method of electron backscatter diffraction (EBSD)

The current analysis generates a broader statistics by using a new tool to analyze the types of nearly all grain boundaries on a standard-sized wafer [13]. It is based on X-ray Laue scans (Laue X-ray diffraction, Laue XRD) performed at optically selected positions. Only one point per grain positioned at the most centered region of the grain is analyzed. Only grains exceeding the size of the 500 µm measuring diameter of the X-ray spot are investigated. By comparing the grain orientation of neighboring grains, the grain boundary types can be determined. The correlation of this information with the spatially resolved lifetime-calibrated photoluminescence (PL) [14-16] images evaluated at grain boundaries of mc-Si wafers after different processing steps, generates a reliable and large statistics of the dependence of lifetime values after the different processing steps on the grain boundary type. The resolution of the PL images in this investigation is 50 µm. In the following, *at a grain boundary* is referred to as the area covered by pixels of a PL image that are crossed by a grain boundary.

Lifetime contrasts and the interstitial Fe concentration [Fe_i] (based on lifetime-calibrated PL images) [17,18] at grain boundaries were determined for all samples after all processing steps.

2 LIFETIME CONTRAST VALUE

The difference between PL intensities at a grain boundary and the intensity in the neighboring grains normalized to the intensity in the grains is usually called PL contrast value [8,12]. As in this analysis the PL images are lifetime-calibrated, a *lifetime* contrast value C_τ is defined analogically:

$$C_\tau = \frac{\tau_{GB} - \tau_0}{\tau_0} \qquad (1)$$

τ_{GB} describes a lifetime value at a grain boundary and τ_0 the average value of two intra-grain plateau lifetime values $\tau_{0,left}$ and $\tau_{0,right}$ positioned on opposite sides of a linescan in the lifetime-calibrated PL image crossing the analyzed point on the grain boundary.

In this investigation contrast values were only calculated for grain boundary points, where the absolute difference of the two plateau lifetime values normalized by τ_0 was less than 20%. Otherwise no lifetime contrast value was determined at these points. The exact

Karzel et al.

procedure of identifying $\tau_{0,left}$ and $\tau_{0,right}$ is described in [19]. Since contrast values from two or even three PL images after different processing steps shall be compared in this analysis, the described requirements need to be fulfilled by all PL images together at the same position on a grain boundary for an indication of lifetime contrast values.

Note that the lifetime contrast depends on the generation rate [12]. In this investigation all PL measurements were taken at a generation rate of $G=1.75 \cdot 10^{17}$ s^{-1}cm^{-2}.

3 EXPERIMENT

Three vertically directly neighboring mc-Si wafers (B doped, 1.5 Ωcm, 156x156 mm^2, 200 μm) with very similar grain structure from mid ingot height of two ingots of different solar-grade quality were cut into samples of 50x50 mm^2. With the expression *solar-grade* we refer here and in the following not to the electronic-grade quality Si feed-stock, but to the conditions of crystallization. The Gen1 sized ingots were produced within the research cluster "SolarWinS" under different conditions:

- Ingot 1: standard solar-grade crucible for mc-Si
- Ingot 2: crucible of high purity fused silica plates

A more detailed description of the properties of the ingots can be found in [19]. Ingot 1 and an ingot similar to ingot 2 are also characterized in [20]. The three neighboring samples of one ingot were arranged in three groups distinguished by different processing steps:

- Group A: only P-gettering and emitter removal
- Group B: POCl$_3$ diffusion with subsequent deposition (both surfaces) and firing of PECVD SiN$_x$:H layers and terminal removal of those layers and the emitter
- Group C: deposition (both surfaces), firing and removal of PECVD SiN$_x$:H layers only

A process flow of the experiment is shown in Fig. 1. The character of most of the grain boundaries of the entire area of the samples was analyzed according to the procedure described in [13] and [19]. The surface passivation with quinhydrone-methanol was performed as described in [21-24]. The minority charge carrier lifetime of all samples was measured by the quasi-steady state photoconductance method (QSSPC) [25], PL images [14] with a resolution of 50 μm were taken and lifetime was calibrated [15,17,18].

A second lifetime measurement using QSSPC and PL was carried out after illuminating the samples until all FeB pairs were dissociated as described in [24].

Samples from group A and group B were treated with a POCl$_3$ diffusion (50 Ω/□) and a P-glass etch in diluted HF(2%). The emitter of samples from group A was taken off during a chemical polishing etch removing 5 μm from each surface.

On both sides of samples from group B and group C 75 nm thick SiN$_x$:H layers were deposited by PECVD. These samples were fired in a belt furnace (peak temperature approximately 700°C) to hydrogenate them. Afterwards the SiN$_x$:H layers were etched off in HF(12.5%) and the emitters of samples from group B
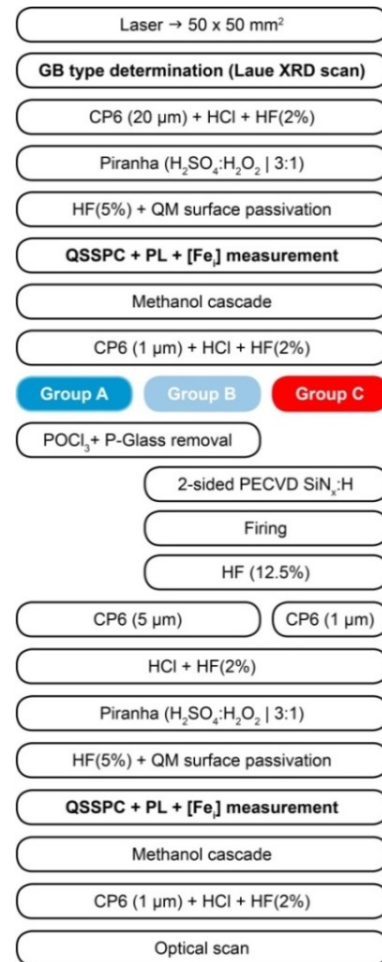
Figure 1: Processing of mc-Si samples (B doped, 1.5 Ωcm, 156x156 mm^2, 200 μm).

were removed. From the surfaces of samples from group C 1 μm was removed to achieve the same surface conditions for all samples.

Again lifetime and [Fe$_i$] were determined by QSSPC and PLI. After cleaning the samples, optical scan images of all samples were taken.

A computer-supported spatial correlation of all lifetime-calibrated PL images of neighboring samples was accomplished. Very small deviations of the grain boundary positions are possible since for a part of the investigation (group A/B) neighboring samples were used.

As described in section 2, for data points on the grain boundaries fulfilling the requested conditions contrast values were determined. [Fe$_i$] maps were calculated from the two lifetime-calibrated PL images before and after dissociating FeB pairs by illumination.

4 RESULTS

In Fig. 2 spatially exactly correlated lifetime-calibrated PL images of a mc-Si sample from ingot 2 as-cut (top), after P-gettering and both-sided emitter removal (center) and a neighboring sample with very similar grain structure and very similar as-cut lifetime distribution after P-gettering and hydrogenation (bottom) are shown. On the left hand side of the images the

arithmetic averages of the lifetime values of these three lifetime maps are given. Comparing the images after $POCl_3$ diffusion and after $POCl_3$ diffusion with subsequent hydrogenation shows, that the recombination activity at some grain boundaries is strongly reduced after firing, while for others it is still high compared to bordering grains. This is a further motivation for grain boundary type specific investigations of the changes in lifetime.

In the top image the as-cut lifetimes are correlated with the different grain boundary types (colored line grid) that were determined from Laue XRD. At some grain boundaries the grain boundary type could not be determined correctly, because the grain size of the adjacent grains was smaller than 500 µm (diameter of the X-ray spot) or because the optical determination of the grain positions did not work out and the grain boundary type calculation was performed with orientations of grains without a common grain boundary. The different types are marked by different colors. The white frames on the colored lines mark positions, where lifetime contrasts could be calculated. Random angle (RA) grain boundaries cannot be classified as CSL grain boundaries and are marked by purple lines. At all these colored marks at the grain boundaries in all three lifetime-calibrated PL images the lifetimes values were analyzed. The lifetime statistics for one grain boundary type is formed by up to 6000 points. This analysis was analogically carried out for the directly neighboring sample of group C, which was directly hydrogenated without previous $POCl_3$ diffusion.

4.1 Lifetime values at different grain boundary types as-cut, after P-gettering and/or SiN$_x$:H firing

The minority charge carrier lifetime values at different grain boundary types in mc-Si samples from ingot 1 and 2 are shown in Fig. 3. Results of samples from group A/B are presented in subfigures a and b and the ones of samples from group C are presented in subfigures c and d.

Values of different grain boundary types are separated by vertical lines into segments in all graphs. The box plots in one segment belong to different processes. In subfigures a and b the black left box plot shows the lifetime value statistics at grain boundaries of the particular grain boundary type of the as-cut sample (group A). The red center box plot displays lifetime values at the according grain boundary type after $POCl_3$ diffusion of the same sample, the blue right box plot gives these values on a neighboring sample after $POCl_3$ diffusion and hydrogenation (group B). The medians, 25 and 75 percentiles are marked by horizontal bars, the arithmetic average values by black dots. The values in brackets on top of the graph show the number of analyzed data points per sample for the particular grain boundary type. Fig. 2 shows the PL images and grain boundaries where the values after different processes presented in Fig. 3b were taken from.

All lifetime values at grain boundaries after the processes in the samples from ingot 2 (Fig. 3b and d) are higher than the ones in the samples from ingot 1 (Fig. 3a and c). This can be explained by the lower concentration of impurities in the whole ingot. To verify this assumption, inductively coupled plasma mass spectrometry (ICP-MS) [26,27] measurements were performed in samples from positions close to the ones the lifetime samples were taken from. The results published
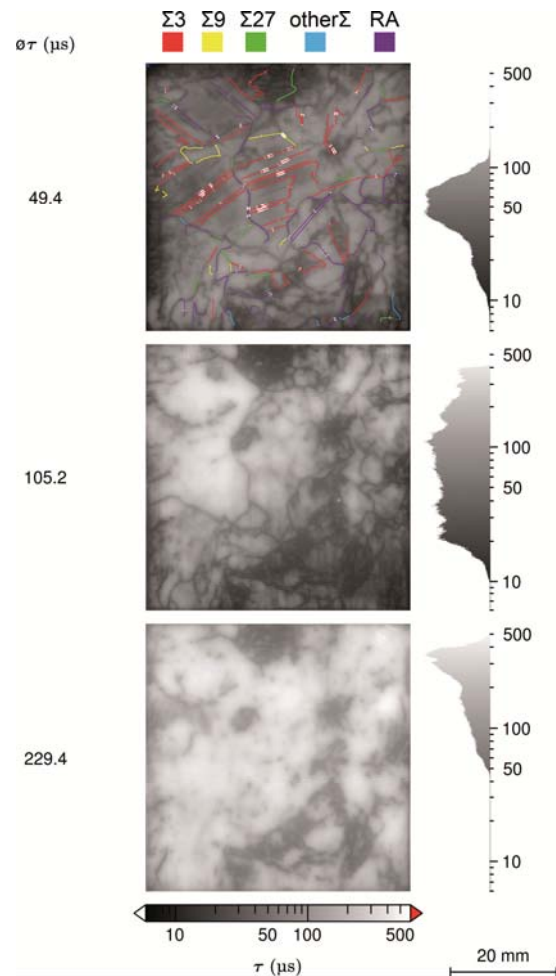
Figure 2: Spatially correlated lifetime-calibrated PL images of mc-Si samples from ingot 2. Top and center: same sample after different processing steps (as-cut, top, and after $POCl_3$, center). Bottom: directly neighboring sample after P-gettering and SiN$_x$:H firing. Average lifetime values after different processing steps shown on the left hand side. The different grain boundary types are marked with different colors in the top image.

in [19] show that the concentrations of nearly all kind of impurities are higher in ingot 1 than in ingot 3 at the investigated position in the ingots.

The median lifetime values of the cleaner samples from ingot 3 displayed in Fig. 3b show a clear trend after the applied processes for all CSL grain boundary types. The as-cut medians are nearly equal for all grain boundary types, but the improvements of the lifetime medians after the processing steps show a dependence on the grain boundary types.

The comparison of median lifetime values of grain boundaries with different CSL grain boundary types after the same processing steps based on broad statistics shows that a higher CSL value leads to lower lifetimes. This is true both for lifetimes after $POCl_3$ diffusion and after $POCl_3$ diffusion and hydrogenation. This fact correlates very well with the trend of stronger decoration of grain boundaries with metal impurities with higher CSL indexes [3].

Data of the only sample that does not completely follow this trend is shown in Fig. 3a. Surprisingly, the median lifetime values at RA grain boundaries after

Karzel et al.

$POCl_3$ diffusion and hydrogenation are slightly higher than at $\sum 27$ grain boundaries for all presented samples. This observation cannot be explained yet and does not fit into the observed trends for CSL grain boundaries. From the higher impurity decoration [3] and the higher degree of misorientation, lower median lifetime values would be expected at RA grain boundaries. A possible statistical explanation for this observation is discussed further in section 5.

The evolution of the median lifetimes after the different processing steps separated by grain boundary types reveals in all graphs of Fig. 3 a continuous
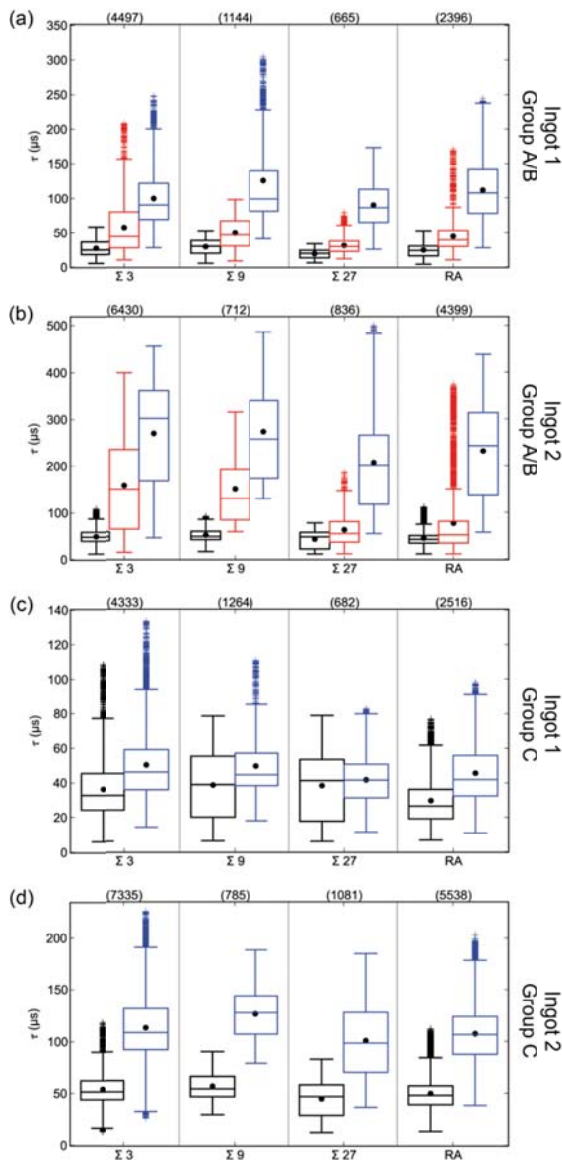
Figure 3: Boxplots of lifetime values at different grain boundary types in mc-Si samples after different processes. (a)+(b) *left* (black): as-cut, *center* (red): after P-gettering, *right* (blue): after P-gettering and hydrogenation; (c)+(d) *left* (black): as-cut, *right* (blue): after hydrogenation. The arithmetic averages are marked by black dots. The number of analyzed data points per grain boundary type is given in brackets. (a)+(c) show data of neighboring samples (group A/B+C, respectively) from ingot 1, and (b)+(d) from ingot 2.

improvement of lifetimes after the applied processes. According to literature [5] a lifetime decrease at grain boundaries after P-gettering was expected. This could not be observed in the analyzed samples.

Fig. 3c and 3d present the lifetime results for neighboring samples that did not receive a $POCl_3$ diffusion, but were hydrogenated directly. The data is arranged analogically to Fig. 3a and b, with the difference, that the black box plots in the segments to the left show the as-cut lifetime values at the corresponding grain boundary types and the blue box plots to the right give the lifetime statistics after hydrogenation. The lifetime images belonging to this statistics are not presented.

Again, the as-cut values are comparable at all grain boundary types. At all grain boundaries the lifetime values improved after hydrogenation. The best median lifetime values after hydrogenation were observed at $\sum 3$ grain boundaries for all analyzed samples, except for the sample from ingot 2 (Fig. 3d), where the best median results were found at $\sum 9$ grain boundaries (the best overall lifetime values after direct hydrogenation are still found at $\sum 3$ grain boundaries for all analyzed samples). Therefore it can be stated again that the median lifetime values at grain boundaries are inversely correlated to the height of the CSL grain boundary type index. Again, the values at the RA grain boundaries do not fit completely into this trend. The lifetime values of the directly hydrogenated samples after hydrogenation are much lower at all grain boundaries compared to the values of very similar neighboring $POCl_3$ gettered samples (Fig. 3a and b).
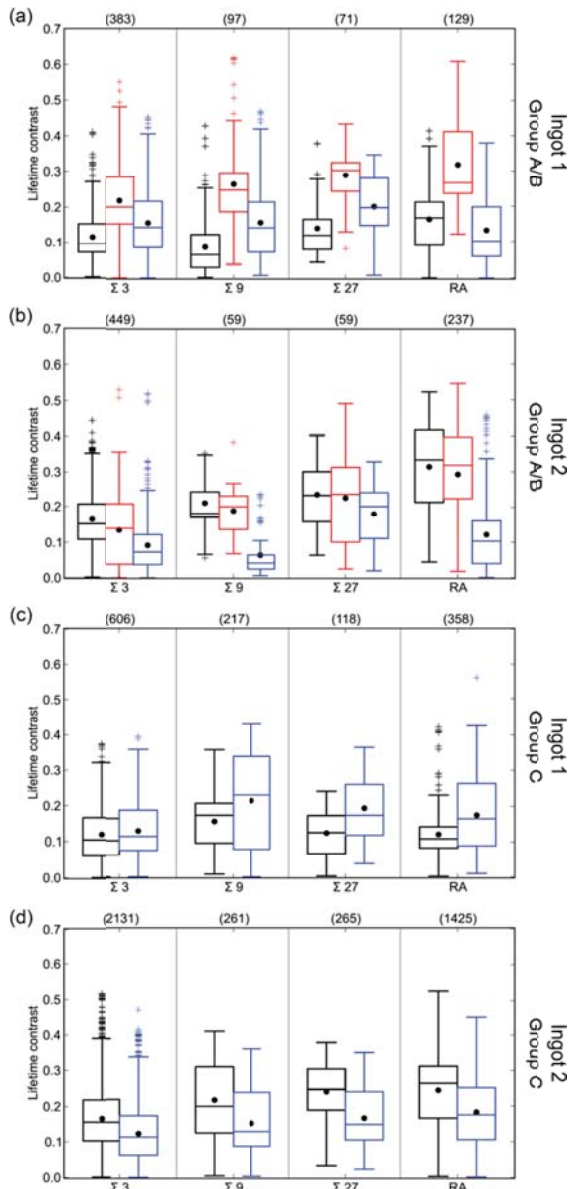
4.2 Lifetime contrast values at different grain boundary types as-cut, after P-gettering and/or SiN_x:H firing

The results of section 4.1 show, that lifetimes at CSL grain boundaries generally increase after the different processing steps. But, as Fig. 2 demonstrates, the lifetime values in the grains also increase. To evaluate if the recombination activity of a grain boundary has been sufficiently passivated or is still harmful compared to neighboring grains, the lifetime at the grain boundary has to be compared to the lifetime in the bordering grains by calculating lifetime contrast values (see section 2).

These lifetime contrasts were calculated (Eq. 1) for points on the grain boundaries marked with white frames around colored lines in Fig. 2. The corresponding data is shown in Fig. 4. Plots of lifetime contrast data from the same samples as presented in Fig. 3 are arranged analogically.

Compared to the lifetime data, the results are different when the recombination activities at grain boundaries are evaluated in terms of lifetime contrasts. The influence of a $POCl_3$ diffusion to lifetime contrasts is demonstrated by the red box plots in Fig. 4a and b. After P-gettering of the sample from ingot 1 the median lifetime contrast values for all CSL grain boundary types increase as expected from literature [4,5], showing that an analysis based on the calculations of lifetime contrast values leads to further important information not accessible from the lifetime values shown in Fig. 3. The relation between impurity concentration at grain boundaries and the concentration in bordering grains is enhanced due to P-gettering because under the influence of the applied temperature during a $POCl_3$ diffusion internal gettering of impurities at grain boundaries can occur.

Karzel et al.

The median lifetime contrast values of the cleaner sample from ingot 2 (Fig. 4b) behave differently after $POCl_3$ diffusion: at $\sum 3$ and RA grain boundaries they even decrease slightly, the increase at the other CSL grain boundary types is very small. The behavior of the two different materials in terms of lifetime contrast values is even more opposed after P-gettering and subsequent firing of SiN_x:H layers (blue boxes on the right in the different segments). The median lifetime contrast values after all processes do not reach the as-cut lifetime contrast values for none of the CSL grain boundary types in material from ingot 1, while these values are significantly below the as-cut lifetime contrast

for the sample from ingot 2. The lifetime contrasts values for the sample from ingot 2 are all lower than the ones of the sample from ingot 1. This can be explained by the different concentrations of impurities (ICP-MS results). A higher concentration of impurity atoms or precipitates at the grain boundaries after P-gettering reduces the efficacy of hydrogenation in reducing the recombination activity.

For all samples and grain boundary types the lifetime contrast values after hydrogenation are lower than the ones after $POCl_3$ diffusion. This means, that hydrogenation is more beneficial at grain boundaries than in grains. This observation is in accordance with results reported earlier [28].
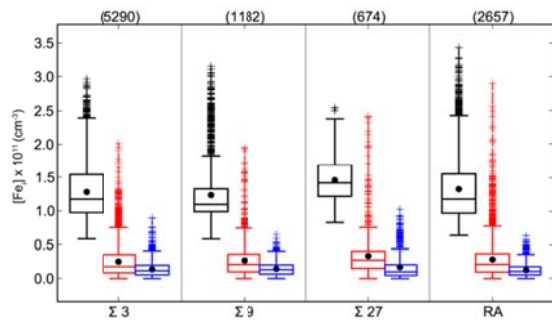
A comparison of the median lifetime contrast values of one sample after the same processing steps at different grain boundary types reveals a dependence on the CSL grain boundary type: higher CSL grain boundary indexes seem to cause higher lifetime contrast values. An exception is the sample from ingot 3 that shows a small deviation from this trend for lifetime contrast values after P-gettering and hydrogenation at $\sum 9$ grain boundaries (Fig. 4b).

The fact that the different materials react differently to the applied processing steps is very clearly noticeable for the samples from group C that were hydrogenated directly without former $POCl_3$ diffusion. The lifetime contrasts for the samples from ingots 1 and 2 are shown in Fig. 4c and d, respectively. After hydrogenation, the lifetime contrasts decrease in the cleaner sample (d), but increase in the sample from ingot 1 (c). Again, this could be explained by internal gettering of the grain boundaries. During the deposition of the SiN_x:H layers at 450°C for approximately 2 h, for example, interstitial iron is known to form precipitates [29,30]. Grain boundaries are preferential sites where precipitates can form [3]. Such processes could lead to a stronger decoration of grain boundaries in the more contaminated material from ingot 1. The less contaminated grain boundaries of samples from ingot 3 could be better passivated by hydrogenation.

4.3 [Fe$_i$] at different grain boundary types as-cut, after P-gettering and SiN_x:H firing

In sections 4.2 and 4.3 a dependency of the minority charge carrier lifetimes at grain boundaries on the grain boundary type was observed. Because the interstitial iron concentration [Fe$_i$] influences lifetimes in mc-Si significantly it was measured before and after the processes for all samples as described in section 3 and the [Fe$_i$] at the grain boundaries was analyzed analogically to the lifetimes as in section 4.1.

In Fig. 5 the results for samples from group A and group B from ingot 1 (compare Fig. 3a) are shown. Because all other box plots for the [Fe$_i$] results look similar, only this one is presented. No dependence on the CSL grain boundary types for the [Fe$_i$] after the processes is found. It is shown based on broad statistics, that [Fe$_i$] is very similar for the different grain boundary types after P-gettering and after P-gettering and hydrogenation, independently of the CSL type. The [Fe$_i$] decreases after the different processing steps, but in the same way for all CSL grain boundaries. Based on broad statistics, the results of Bertoni et al. [6] could be confirmed: [Fe$_i$] is not responsible for the dependence of lifetime values at grain boundaries on the CSL grain boundary type.

Figure 4: Boxplots of lifetime contrast values at different grain boundary types in mc-Si samples after different processes. (a)+(b) *left* (black): as-cut, *center* (red): after P-gettering, *right* (blue): after P-gettering and hydrogenation; (c)+(d) *left* (black): as-cut, *right* (blue): after hydrogenation. The number of analyzed data points per grain boundary type is given in brackets. (a)+(c) show data of neighboring samples (group A/B+C, respectively) from ingot 1, and (b)+(d) from ingot 3.

Figure 5: Boxplots of interstitial iron concentrations at different grain boundary types in neighboring mc-Si samples from ingot 1 after different processes. *left* (black): as-cut, *center* (red): after P-gettering, *right* (blue): after P-gettering and hydrogenation. The number of analyzed data points per grain boundary type is given in brackets.

5 STATISTICAL RELEVANCE

The statistical relevance and reliability of the results shall be discussed in the following.

The effective lifetimes at grain boundaries after the different processes can be influenced by minority charge carriers diffusing towards the grain boundaries from bordering grains, where more carriers were injected. In this case the excess charge carrier density at the grain boundaries increases, resulting in higher effective lifetimes ($\tau = \Delta n / G$ [15]). This effect is supposed to be higher for samples with longer minority charge carrier diffusion lengths within the grain. After hydrogenation the diffusion lengths should be longer. That is why this analysis does not evaluate the change in lifetimes at grain boundaries quantitatively (because it is influenced by the changes in the adjacent grains as well), but reflects the situations at the grain boundaries close to reality, where a solar cell is illuminated homogeneously by the sun.

Regarding the statistics it has to be taken into consideration that the analyzed data points at one grain boundary should exhibit very similar properties and that it is more important to analyze many different grain boundaries of one CSL type than to analyze many points at one grain boundary. The small deviations from the observed trends might be explained by this detail. Nevertheless, as shown in Fig. 2, the analyzed amount of spatially separated grain boundaries from all types are still significant. Many further samples that were not taken into this publication were analyzed by the described analysis method, and all these results of further investigations confirm the described trends.

The maximum normalized difference of plateau lifetime values at the two sides of grain boundaries was accepted to be 20%. The trend of the results in the presented graphs does not change at all, when this limit is decreased to 10%. Simply the number of analyzed data points is slightly smaller.

The character of grain boundaries is not completely determined by its CSL index, that only describes the orientation of the bordering grains. The position and orientation of the common surface of the two grains is not determined by this classification. However, it is very probable that there exist preferential surface orientations and that the CSL indexes are correlated to certain surface orientations.

6 SUMMARY

A broad statistics shows, that the minority charge carrier lifetimes at grain boundaries in mc-Si after P-gettering and/or SiN_x:H firing depend on the CSL grain boundary type: higher CSL indexes are correlated with lower lifetimes.

In contrast to formerly reported results [5], no lifetime decrease at grain boundaries after P-gettering could be found. However, an increase of lifetime contrast values was detected for all grain boundary types in standard solar-grade material (ingot 1). For higher CSL indexes the increase was stronger. After subsequent hydrogenation of this material the lifetime contrast values still were higher than the as-cut levels. Again higher values were correlated with higher CSL indexes.

A different evolution of lifetime contrast values after the different processes was shown by the cleaner material. The values of samples from ingot 2 decreased both after P-gettering and after direct hydrogenation.

Many results of this investigation indicate that hydrogenation of cleaner grains and grain boundaries is more efficient. An explanation of this fact could be, that impurities at grain boundaries in form of atoms or precipitates hinder the passivation of dangling bonds by atomic hydrogen during SiN_x:H firing.

Generally, a good correlation between CSL grain boundary types and lifetimes at grain boundaries was observed. No dependency of the $[Fe_i]$ on the CSL grain boundary type could be found, indicating that the reason for the observed dependency on the grain boundary type rather could correlate with the dependency of dislocation density with the CSL grain boundary type, as formerly reported [6].

7 ACKNOWLEDGMENTS

8 REFERENCES

[1] J. Tan, A. Cuevas, D. Macdonald, T. Trupke, R. Bardos, and K. Roth, Progress in Photovoltaics: Research and Applications 16, 129 (2008).

[2] G. Hahn, M. Käs, and B. Herzog, Solid State Phenomena 156-158, 343 (2010).

[3] T. Buonassisi, A. Istratov, S. Peters, C. Ballif, J. Isenberg, S. Riepe, W. Warta, R. Schindler, G. Willeke, Z. Cai, B. Lai, and E. Weber, Applied Physics Letters 87, 121918 (2005).

[4] A. Liu, Y. Fan, and D. Macdonald, Progress in Photovoltaics: Research and Applications 19, 649 (2011).

[5] L. Geerligs, Y. Komatsu, I. Röver, K. Wambach, I. Yamaga, and T. Saitoh, Journal of Applied

Physics 102, 093702 (2007).

[6] M. Bertoni, S. Hudelson, B. Newman, D. Fenning, H. Dekkers, E. Cornagliotti, A. Zuschlag, G. Micard, G. Hahn, G. Coletti, B. Lai, and T. Buonassisi, Progress in Photovoltaics: Research and Applications 19, 187 (2011).

[7] A. Fedotov, A. Mazanik, and A. Ulyashin, Solar Energy Materials & Solar Cells 72, 589 (2002).

[8] J. Chen, T. Sekiguchi, D. Yang, F. Yin, K. Kido, and S. Tsurekawa, Journal of Applied Physics 96, 5490 (2004).

[9] J. Chen, D. Yang, Z. Xi, and T. Sekiguchi, Physica B: Condensed Matter 364, 162 (2005).

[10] M. Rinio, M. Kaes, G. Hahn, and D. Borchert, in Proceedings of the 21st European Photovoltaic Solar Energy Conference, Dresden, 4-8 Sep 2006, pp. 684–687.

[11] J. Junge, A. Herguth, S. Seren, and G. Hahn, in Proceedings of the 24th European Photovoltaic Solar Energy Conference, Hamburg, 21-25 Sep 2009, pp. 1131–1136.

[12] H. Sio, T. Trupke, S. Phang, and D. Macdonald, in Proceedings of the 27th European Photovoltaic Solar Energy Conference, Frankfurt, 24-29 Sep 2012, pp. 714–718.

[13] C. Reimann, E. Meissner, M. Trempa, T. Lehmann, T. Geiger, M. Knetzger, M. Zschorsch, and J. Friedrich, in Proceedings of the 5th International Workshop on Crystalline Silicon Solar Cells, Boston, 1-3 Nov 2011 (2011)

[14] T. Trupke, R. Bardos, M. Schubert, and W. Warta, Applied Physics Letters 89, 044107 (2006).

[15] S. Herlufsen, J. Schmidt, D. Hinken, K. Bothe, and R. Brendel, Physica Status Solidi (RRL) - Rapid Research Letters 2, 245 (2008).

[16] D. Macdonald, J. Tan, and T. Trupke, Journal of Applied Physics 103, 073710 (2008).

[17] D. Macdonald, L. Geerligs, and A. Azzizi, Journal of Applied Physics 95, 1021 (2004).

[18] D. Macdonald, T. Roth, P. Deenapanray, T. Trupke, and R. Bardos, Applied Physics Letters 89, 142107 (2006).

[19] P. Karzel, M. Ackermann, L. Gröner, C. Reimann, M. Zschorsch, S. Meyer, Journal of Applied Physics, to be published.

[20] W. Kwapil. A. Zuschlag, I. Reis, I. Schwirtlich, S. Meyer, R. Zierer, R. Krain, F. Kießling, M. Schumann, C. Schmid, S. Riepe, in Proceedings of the 27th European Photovoltaic Solar Energy Conference, Frankfurt, 24-29 Sep 2012, pp. 627–635.

[21] H. Takato, I. Sakata, and R. Shimokawa, Japanese Journal of applied Physics 41, L 870 (2002).

[22] B. Chhabra, S. Bowden, R. Opila, and C. Honsberg, Applied Physics Letters 96, 063502 (2010).

[23] K. Pollock, J. Junge, and G. Hahn, IEEE Journal of Photovoltaics 2, 1 (2012).

[24] P. Karzel, A. Frey, S. Fritz, and G. Hahn, Journal of Applied Physics 113, 114903 (2013).

[25] R. Sinton and A. Cuevas, Applied Physics Letters 69, 2510 (1996).

[26] R. Houk, V. Fassel, D. Flesch, A. Gray, and E. Taylor, Analytical Chemistry 52(14), 2283 (1980).

[27] S. Nelms, *Inductively coupled plasma mass spectrometry handbook*, 4th ed. (Blackwell Publishing, Oxford, 2005).

[28] M. Rinio, A. Hauser, and H. Möller, in Proceedings of the 3rd World Conference on Photovoltaic Energy Conversion, Osaka, 11-18 May 2003 (IEEE, New York, 2003) pp. 112–115

[29] A. Haarahiltunen, H. Väinölä, O. Anttila, M. Yli-Koski, and J. Sinkkonen, Journal of Applied Physics 101, 043507 (2007).

[30] R. Krain, S. Herlufsen, and J. Schmidt, Applied Physics Letters 93, 152108 (2008).

Karzel et al.